Color dipoles and ρ, ϕ electroproduction

J. R. Forshaw
Department of Physics and Astronomy, University of Manchester, Manchester M13 9PL, England

R. Sandapen
Department of Physics and Astronomy, University of Manchester, Manchester M13 9PL, England
and Department of Physics, Engineering Physics and Optics, Laval University, Quebec, Canada G1K 7P4

G. Shaw
Department of Physics and Astronomy, University of Manchester, Manchester M13 9PL, England

(Received 16 December 2003; published 20 May 2004)

We present a detailed comparison of a variety of predictions for diffractive light vector meson production with the data collected at the DESY HERA collider. All our calculations are performed within a dipole model framework and make use of different models for the meson light-cone wave function. There are no free parameters in any of the scenarios we consider. Generally we find good agreement with the data using rather simple Gaussian motivated wave functions in conjunction with dipole cross sections which have been fitted to other data.

DOI: 10.1103/PhysRevD.69.094013 PACS number(s): 12.40.Nn, 13.60.Le

I. INTRODUCTION

In a previous paper, Forshaw, Kerley, and Shaw (FKS) [1] reported on a successful attempt to extract the cross section for scattering color dipoles of fixed transverse size off protons using both electroproduction and photoproduction γp total cross section data, together with the constraint provided by the measured ratio of the diffraction dissociation cross section to the total cross section for real photons. Subsequently, the same model has been applied to ''diffractive deep inelastic scattering'' (DDIS) $\gamma^* p \to Xp$ [2] and also to deeply virtual Compton scattering (DVCS) $\gamma^* p \to \gamma p$ [3]. In both cases, the model was shown to yield predictions in agreement with the data [4,5] with no adjustable parameters. The model can also be extended to diffractive vector meson production:

$$\gamma^*(q) + p(p) \to V(q') + p(p'), \quad V = \rho, \phi \text{ or } J/\Psi, \tag{1}$$

where the squared center of mass energy $s = W^2 = (p+q)^2 \gg Q^2, M_V^2$. In these processes the choice of vector meson, as well as of different photon virtualities, allows one to explore contributions from dipoles of different transverse sizes. The process also has the advantage that there is a wide range of available data. It ought also to provide important information on the poorly known light-cone wave functions of the vector mesons.

The aim of this paper is to confront the predictions of the dipole model with the DESY *ep* collider HERA data on ρ and ϕ electroproduction. The predictions for J/ψ production are best considered in conjunction with an analysis of open charm production, and will be discussed elsewhere. We shall focus on the FKS model [1], but we also compare with the predictions of two other models: the Golec-Biernat–Wüsthoff (GW) saturation model [6,7] and the recent ''Color Glass Condensate'' (CGC) model of Iancu, Itakura and Munier [8]. For the meson light-cone wave function, we shall consider three different ansätze: the Dosch, Gousset, Kulzinger and Pirner (DGKP) [9] model; the Nemchik, Nikolaev, Predazzi and Zakharov (NNPZ) [10] model; and a simple ''boosted Gaussian'' wave function, which can be considered as a special case of the latter.

The paper is laid out as follows. In the first two sections we summarize the dipole models used and discuss the forms chosen for the vector meson wave functions. We then compare their predictions with experiment before drawing our conclusions.

II. THE COLOR DIPOLE MODEL

In the color dipole model [11], the eigenstates of the scattering (diffraction) operator are ''color dipoles,'' i.e., quark-antiquark pairs of transverse size r in which the quark carries a fraction z of the photon's light-cone momentum.[1] In the proton's rest frame, the formation of the dipole occurs on a time scale far longer than that of its interaction with the target proton. Because of this, the forward imaginary amplitude for singly diffractive photoprocesses $\gamma p \to Xp$ is assumed to factorize into a product of light-cone wave functions associated with the initial and final state particles γ and X and a universal dipole cross section $\hat{\sigma}(s,r)$, which contains all the dynamics of the interaction of the $q\bar{q}$ dipole with the target proton. In particular for reaction (1) one obtains

$$\mathrm{Im}\mathcal{A}(s,t=0) = s \sum_{h,\bar{h}} \int d^2\mathbf{r} dz \Psi^{\gamma}_{h,\bar{h}}(r,z) \hat{\sigma}(s,r) \Psi^{V*}_{h,\bar{h}}(r,z), \tag{2}$$

[1] We work in light-cone coordinates $x^\mu = (x^+, x^-, \boldsymbol{x})$ in the convention where $x^\pm = x^0 \pm x^3$. Here $z = k^+/q^+$ where the momentum k of the quark is $(k^+, k^-, \boldsymbol{k})$.

TABLE I. Parameters for the FKS model [3] in appropriate GeV based units.

λ_S	0.06 ± 0.01	λ_H	0.44 ± 0.01
a_0^S	30.0(fixed)	a_2^H	0.072 ± 0.010
a_4^S	0.027 ± 0.007	a_6^H	1.89 ± 0.03
		ν_H	3.27 ± 0.01
B	7.05 ± 0.08	c^2	0.20 (fixed)
R	6.84 ± 0.02		
$m_{u,d,s}^2$	0.08 (fixed)	m_c^2	1.4 (fixed)

where $\Psi^{\gamma}_{h,\bar{h}}(r,z)$ and $\Psi^{V}_{h,\bar{h}}(r,z)$ are the light-cone wave functions of the photon and vector meson, respectively. The quark and antiquark helicities are labeled by h and $\bar{h}$ and we have suppressed reference to the meson and photon helicities. The dipole cross section is usually assumed to be flavor independent[2] and, as implied by our notation, ''geometric,'' i.e. for a given s, it is assumed to depend on the transverse dipole size, but not the light-cone momentum fraction z. The light-cone wave functions do depend on the quark flavor via their charges and masses. Finally, the corresponding real part of the amplitude (2) is either neglected or, as here, is estimated using analyticity.

While the photon light-cone wave function can be calculated within perturbation theory, at least for small dipole sizes, the vector meson light-cone wave functions are not reliably known, and must be obtained from models. This will be discussed in the following section. The rest of this section is devoted to the dipole cross section, for which we shall consider three different models.[3] Since full details are given in the original papers, our treatment will be brief.

A. The FKS model

The FKS model [1–3] is a two-component model

$$\hat{\sigma}(s,r) = \hat{\sigma}_{\rm soft}(s,r) + \hat{\sigma}_{\rm hard}(s,r), \tag{3}$$

in which each term has a Regge type energy dependence on the dimensionless energy variable $r^2 s$:

$$\hat{\sigma}_{\rm soft}(s,r) = a_0^S \left(1 - \frac{1}{1 + a_4^S r^4} \right) (r^2 s)^{\lambda_S}, \tag{4}$$

$$\hat{\sigma}_{\rm hard}(s,r) = (a_2^H r^2 + a_6^H r^6) \exp(-\nu_H r) (r^2 s)^{\lambda_H}. \tag{5}$$

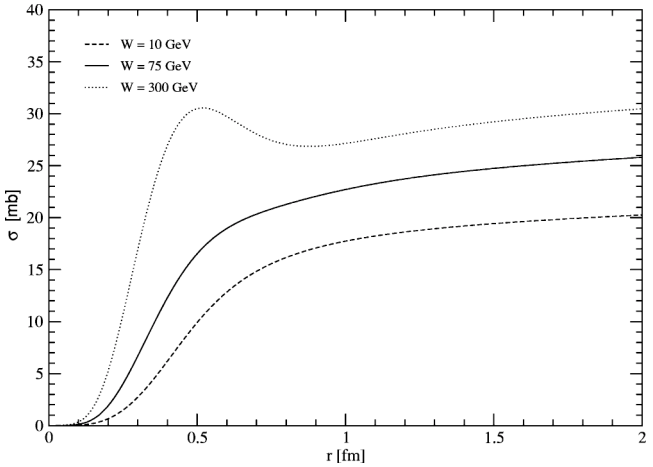

FIG. 1. The FKS dipole cross section at $W = 10, 75, 300$ GeV.

This parametric form[4] is chosen so that the hard term dominates at small r and goes to zero like r^2 as $r \to 0$ in accordance with ideas of color transparency, while the soft term dominates at larger $r \approx 1$ fm, with a hadron-like soft Pomeron behavior. In addition, to allow for possible confinement effects in the photon wave function at large r, FKS modified the perturbative wave functions $\psi^0_{T,L}(r,z)$ by multiplying them by an adjustable Gaussian enhancement factor:

$$|\psi_{T,L}(r,z)|^2 = |\psi^0_{T,L}(r,z)|^2 f(r), \tag{6}$$

where

$$f(r) = \frac{1 + B \exp[-c^2 (r-R)^2]}{1 + B \exp(-c^2 R^2)}. \tag{7}$$

This behavior is qualitatively suggested by an analysis [13] of the scattering eigenstates in a generalized vector dominance model [14] which provides a good description of the soft Pomeron contribution to the nucleon structure function F_2 on both protons and nuclei [15].[5] The free parameters in both the dipole cross section and the photon wave function were then determined by a fit to structure function and real photoabsorption data. The resulting values are given in Table I. Having been obtained in this way, they were then used to predict successfully the cross sections for other processes which depend solely on the dipole cross section and the photon wave function, namely diffractive deep inelastic scattering (DDIS) [2] and deeply virtual Compton scattering (DVCS) [3].

The resulting dipole cross section is shown in Fig. 1. As can be seen, as s increases the dipole cross section grows most rapidly for small r, where the hard term dominates, eventually exceeding the typically hadronic cross section found for dipoles of large $r \approx 1$ fm. This rise could well be

[2]For the GW model, this is only strictly so at large Q^2 since some flavor dependence enters indirectly at small Q^2 through the definitions of $x_{\rm mod}$ (see below).

[3]For a more general review of phenomenological dipole models see, for example, [12].

[4]This form, taken from [3], is actually a simplified form of that used in the [1,2], but gives almost identical results.

[5]For a more recent discussion of the relation between GVD models and the dipole approach, see [16].

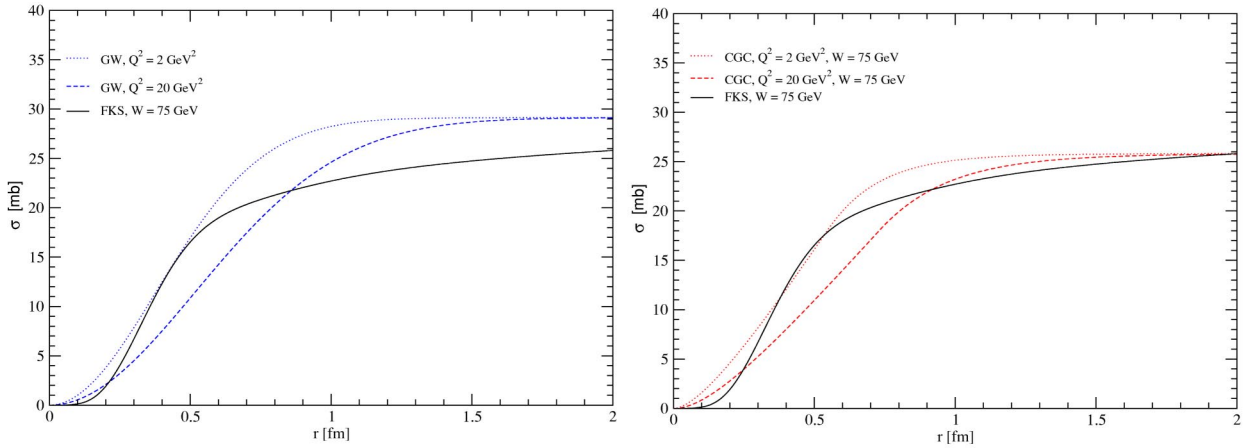

FIG. 2. The GW dipole cross section (left) and CGC dipole cross section (right) at $W=75$ GeV for $Q^2=2$ GeV^2 and $Q^2=20$ GeV^2. The Q^2-independent FKS dipole cross section at the same energy is shown for comparison.

tamed by unitarity or saturation effects [17]. However, the authors have argued [18] that such saturation effects are unlikely to be important until the top of the HERA range and beyond, and they are not included in the FKS model in its present form.

B. The GW model

This well-known model [6,7] combines the approximate behavior $\hat{\sigma}\to r^2 f(x)$ at small r together with a phenomenological saturation effect by adopting the attractively simple parametric form

$$\hat{\sigma}=\sigma_0\left(1-\exp\left[\frac{-r^2Q_0^2}{4(x_{\rm mod}/x_0)^{\lambda}}\right]\right). \tag{8}$$

Here $x_{\rm mod}$ is a modified Bjorken variable,

$$x_{\rm mod}=x\left(1+\frac{4m_f^2}{Q^2}\right), \tag{9}$$

where m_f is the quark mass and $Q_0=1$ GeV. The three free parameters x_0, σ_0 and λ were successfully fitted to F_2 data. The four-flavor fit which we shall use in this paper yielded $\sigma_0=29.12$ mb, $\lambda=0.277$ and $x_0=0.41\times10^{-4}$. The quark masses are chosen to be 0.14 GeV for the light quarks and 1.5 GeV for the charm quark. The model is also able to describe $F_2^{D(3)}$ data [7]. A recent refinement of the model takes into account corrections due to DGLAP evolution at large Q^2 [19], but these are rather small corrections and are not included here. Finally, all these results are obtained with a purely perturbative photon wave function, which is somewhat enhanced at large r values by the use of a lighter quark mass than that used in the FKS model.[6] The resulting behavior of the dipole cross section is illustrated and compared to that of the FKS model in Fig. 2.

[6]See, for example, Fig. 3 of [3].

C. The CGC model

The dipole model of Iancu, Itakura and Munier [8] can be thought of as a development of the Golec-Biernat–Wüsthoff saturation model. Though still largely a phenomenological parametrization, the authors do claim that it contains the main features of the ''color glass condensate'' regime, where the gluon densities are high and non-linear effects become important. In particular, they take

$$\hat{\sigma}=2\pi R^2\mathcal{N}_0\left(\frac{rQ_s}{2}\right)^{2\{\gamma_s+[\ln(2/rQ_s)/\kappa\lambda\ln(1/x)]\}} \quad \text{for} \quad rQ_s\leqslant 2$$

$$=2\pi R^2\{1-\exp[-a\ln^2(brQ_s)]\} \quad \text{for} \quad rQ_s>2, \tag{10}$$

where the saturation scale $Q_s\equiv(x_0/x)^{\lambda/2}$ GeV. The coefficients a and b are uniquely determined by ensuring continuity of the cross section and its first derivative at $rQ_s=2$. The leading order Balitsky, Fadin, Kuraev, and Lipatov (BFKL) equation fixes $\gamma_s=0.63$ and $\kappa=9.9$. The coefficient $\mathcal{N}_0$ is strongly correlated to the definition of the saturation scale and the authors find that the quality of fit to F_2 data is only weakly dependent upon its value. For a fixed value of $\mathcal{N}_0$, there are therefore three parameters which need to be fixed by a fit to the data, i.e. x_0, λ and R. In this paper, we take $N_0=0.7$ and a light quark mass of $m_q=140$ MeV, for which the fit values are $x_0=2.67\times10^{-5}$, $\lambda=0.253$ and $R=0.641$ fm.

As for the GW dipole, we compare to the FKS dipole at two values of Q^2 in Fig. 2.

III. LIGHT-CONE WAVE FUNCTIONS

The light-cone wave functions $\Psi_{h,\bar{h}}(\boldsymbol{r},z)$ in the mixed representation (r,z) used in the dipole model are obtained from a two-dimensional Fourier transform

$$\Psi_{h,\bar{h}}(r,z)=\int\frac{d^2\boldsymbol{k}}{(2\pi)^2}e^{i\boldsymbol{k}\cdot\boldsymbol{r}}\Psi_{h,\bar{h}}(k,z) \tag{11}$$

of the momentum space light-cone wave functions $\Psi_{h,\bar{h}}(k,z)$, where the quark and antiquark are in states of definite helicity, h and $\bar{h}$, respectively. For transversely (T) or longitudinally (L) polarized photons, the momentum space light-cone wave functions themselves are calculated perturbatively [9,20] (per fermion of charge ee_f):

$$\Psi^{\gamma(\lambda)}_{h,\bar{h}}(k,z)=\sqrt{\frac{N_c}{4\pi}}\frac{\bar{u}_h(\boldsymbol{k})}{\sqrt{z}}(ee_f\gamma.\varepsilon^{\lambda}_{\gamma})\frac{v_{\bar{h}}(-\boldsymbol{k})}{\sqrt{1-z}}\Phi^{\gamma}(k,z). \tag{12}$$

Hereafter, λ denotes the polarization state L or T. ε^{λ} are the polarization vectors and the "scalar" part[7] of the photon light-cone wave function Φ^{γ} is given by

$$\Phi^{\gamma}(k,z)=\frac{z(1-z)}{z(1-z)Q^2+k^2+m_f^2}. \tag{13}$$

For the vector mesons, the simplest approach is to assume the same vector current as in the photon case, with an additional (unknown) vertex factor $\Gamma_{\lambda}(k,z)$,

$$\Psi^{V(\lambda)}_{h,\bar{h}}(k,z)=\sqrt{\frac{N_c}{4\pi}}\frac{\bar{u}_h(\boldsymbol{k})}{\sqrt{z}}(\gamma.\varepsilon^{\lambda}_{V})\frac{v_{\bar{h}}(-\boldsymbol{k})}{\sqrt{1-z}}\Phi^{V}_{\lambda}(k,z), \tag{14}$$

where the scalar part of the meson light-cone wave function is given by

$$\Phi^{V}_{\lambda}(k,z)=\frac{z(1-z)\Gamma_{\lambda}(k,z)}{-z(1-z)M_V^2+k^2+m_f^2}. \tag{15}$$

Different models are defined by specifying these scalar wave functions. In practice, it is common to choose the same functional form for Φ^V_T and Φ^V_L; perhaps allowing the numerical parameters to differ.

It is instructive to consider the longitudinal wave functions more explicitly. Using the polarization vectors

$$\varepsilon^L_{\gamma}=\left(\frac{q^+}{Q},\frac{Q}{q^+},\mathbf{0}\right),\quad \varepsilon^L_V=\left(\frac{v^+}{M_V},-\frac{M_V}{v^+},\mathbf{0}\right), \tag{16}$$

and the rules of light-cone perturbation theory given in [20], it follows that the longitudinal photon light-cone wave function is

$$\Psi^{\gamma,L}_{h,\bar{h}}(k,z)=\sqrt{\frac{N_c}{4\pi}}\delta_{h,-\bar{h}}ee_f\left(\frac{2z(1-z)Q}{k^2+m_f^2+z(1-z)Q^2}-\frac{1}{Q}\right) \tag{17}$$

and that of the vector meson is

$$\Psi^{V,L}_{h,\bar{h}}(k,z)=\sqrt{\frac{N_c}{4\pi}}\delta_{h,-\bar{h}}\left(\frac{z(1-z)2M_V\Gamma(k,z)}{k^2+m_f^2-z(1-z)M_V^2}+\frac{\Gamma(k,z)}{M_V}\right). \tag{18}$$

On substituting (17) in (11) the second term of (17) leads to a dipole of vanishing size, which does not contribute to the cross section. This is in accord with gauge invariance. The same argument cannot be used to justify the omission of the second term in the meson wave function (18), since the latter has a k dependence. In practice, this term is omitted in the DGKP model [9], but retained in the NNPZ model [10]. A discussion of the gauge invariance issues surrounding this point can be found in [21].

Before discussing these models more fully, we give the explicit forms for the photon wave functions in r space. The normalized photon light-cone wave functions are [9]

$$\Psi^{L}_{h,\bar{h}}(r,z)=\sqrt{\frac{N_c}{4\pi}}\delta_{h,-\bar{h}}ee_f 2z(1-z)Q\frac{K_0(\epsilon r)}{2\pi}, \tag{19}$$

and

$$\Psi^{T(\gamma=\pm)}_{h,h}(r,z)=\pm\sqrt{\frac{N_c}{2\pi}}ee_f\{ie^{\pm i\theta_r}[z\,\delta_{h\pm,\bar{h}\mp}-(1-z)\,\delta_{h\mp,\bar{h}\pm}]\partial_r+m_f\delta_{h\pm,\bar{h}\pm}\}\frac{K_0(\epsilon r)}{2\pi}, \tag{20}$$

where

$$\epsilon^2=z(1-z)Q^2+m_f^2. \tag{21}$$

Since the modified Bessel function $K_0(x)$ decreases exponentially at large x, these equations imply that at high Q^2, the wave functions are suppressed for large r unless z is close to its end-points values 0 or 1. As can be seen from Eqs. (19) and (20), these end points are suppressed for the longitudinal but not the transverse case. This is the origin of the statement that transverse meson production is more inherently nonperturbative than for longitudinal meson production.

For small r, the perturbative expressions given above are reliable. For large r-values, however, confinement corrections are likely to modify the perturbation theory result. These larger r values contribute significantly at low Q^2, where the wave functions are sensitive to the non-zero quark masses m_f, which prevent the modified Bessel function from diverging in the photoproduction limit. For these reasons, the photon light-cone wave functions at large r are clearly model dependent.

We now turn back to the meson wave functions. These are subject to two constraints. The first is the normalization condition [20,22]

[7]This would indeed be the photon light-cone wave function in a toy model of scalar quarks and photons.

TABLE II. Parameters and normalizations of the DGKP light-cone wave functions in appropriate GeV based units. For the transverse case, the first and second values are for the FKS and GW quark masses, respectively.

DGKP	ω_L	ω_T	$\mathcal{N}_L$	$\mathcal{N}_T$
ρ	0.331	0.206,0.218	15.091	5.573,8.682
ϕ	0.368	0.244,0.262	15.703	5.689,8.000

$$1=\sum_{h,\bar{h}}\int\frac{d^2\boldsymbol{k}}{(2\pi)^2}dz|\Psi^{V(\lambda)}_{h,h}(k,z)|^2$$
$$=\sum_{h,\bar{h}}\int d^2\boldsymbol{r}dz|\Psi^{V(\lambda)}_{h,h}(r,z)|^2, \tag{22}$$

which embodies the assumption that the meson is composed solely of $q\bar{q}$ pairs. Note that this normalization is consistent with Eq. (2) and differs by a factor 4π relative to the conventional light-cone normalization.

The second constraint comes from the electronic decay width [9,22]

$$ef_V M_V\varepsilon^*_\gamma.\varepsilon_V$$
$$=\sum_{h,\bar{h}}\int\frac{d^2\boldsymbol{k}}{(2\pi)^2}\frac{dz}{z(1-z)}[z(1-z)Q^2+k^2+m_f^2]$$
$$\times\Psi^V_{h,\bar{h}}(k,z)\Psi^{\gamma*}_{h,\bar{h}}(k,z), \tag{23}$$

where the coupling f_V of the meson to electromagnetic current can be determined from the experimentally measured leptonic width $\Gamma_{V\to e^+e^-}$ since $3M_V\Gamma_{V\to e^+e^-}=4\pi\alpha^2_{\rm em}f_V^2$. We shall prefer to implement the constraint directly in terms of the r-space wave functions. For our purposes, we can write the meson wave functions in r space as

$$\Psi^{V,L}_{h,\bar{h}}(r,z)=\sqrt{\frac{N_c}{4\pi}}\delta_{h,-\bar{h}}\frac{1}{M_V z(1-z)}$$
$$\times[z(1-z)M_V^2+\delta(m_f^2-\nabla_r^2)]\phi_L(r,z), \tag{24}$$

where $\nabla_r^2\equiv(1/r)\partial_r+\partial_r^2$, and

$$\Psi^{V,T(\gamma=\pm)}_{h,\bar{h}}(r,z)$$
$$=\pm\sqrt{\frac{N_c}{4\pi}}\frac{\sqrt{2}}{z(1-z)}\{ie^{\pm i\theta_r}[z\,\delta_{h\pm,\bar{h}\mp}-(1-z)\,\delta_{h\mp,\bar{h}\pm}]\partial_r$$
$$+m_f\delta_{h\pm,\bar{h}\pm}\}\phi_T(r,z). \tag{25}$$

Note the second term in square brackets which occurs in the longitudinal meson case. This is a direct consequence of keeping the second term in Eq. (18). For the DGKP wave functions this term is absent, i.e. $\delta=0$, whilst NNPZ keep this term, i.e. $\delta=1$. In terms of these wave functions, (23) becomes [assuming that $r\phi_T(r,z)\to 0$ at $r=0$ and $r=\infty$]

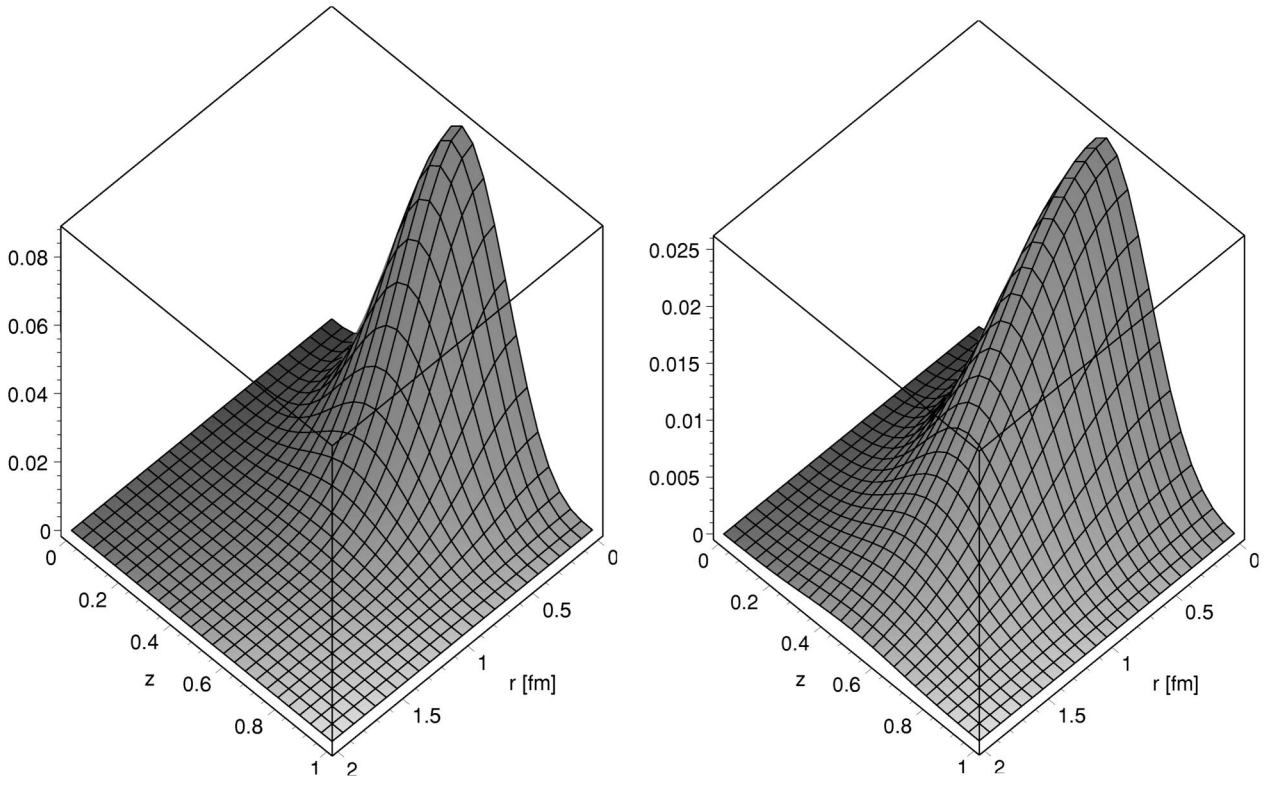

FIG. 3. The ρ wave functions $|\Psi^L|^2$ (left) and $|\Psi^T|^2$ (right) in the DGKP model with the quark mass used in the FKS dipole model. Note the different scales for the ordinate.

$$f_V M_V = \frac{N_c}{\pi}\hat{e}_f \int_0^1 \frac{dz}{z(1-z)} \times [z(1-z)M_V^2 + \delta(m_f^2 - \nabla_r^2)]\phi_L(r,z)|_{r=0} \quad (26)$$

and

$$f_V M_V = -\frac{N_c}{2\pi}\hat{e}_f \int_0^1 \frac{dz}{[z(1-z)]^2} \times [(z^2+(1-z)^2)\nabla_r^2 - m_f^2]\phi_T(r,z)|_{r=0}. \quad (27)$$

In computing f_ϕ and all other observables involving the ϕ meson we in all cases take the quark mass to be equal to the light quark mass plus 150 MeV.

A. DGKP meson wave function

In the DGKP approach [9], the r and z dependences of the wave function are assumed to factorize.[8] Specifically, the scalar wave function is given by[9]

$$\phi_\lambda^V(r,z) = G(r) f_\lambda(z) z(1-z). \quad (28)$$

A Gaussian dependence on r is assumed, that is

$$G(r) = \frac{\pi f_V}{N_c \hat{e}_f M_V} e^{-\omega_\lambda^2 r^2/2}, \quad (29)$$

and $f_\lambda(z)$ is given by the Bauer-Stech-Wirbel model [24]:

$$f_\lambda(z) = \mathcal{N}_\lambda \sqrt{z(1-z)}\, e^{-M_V^2 (z-1/2)^2/2\omega_\lambda^2}. \quad (30)$$

Setting $\delta = 0$ [recall that this is equivalent to neglecting the second term in (18)] in Eq. (24) results in

$$\Psi_{h,\bar{h}}^{V,L}(r,z) = z(1-z)\,\delta_{h,-\bar{h}} \frac{\sqrt{\pi} f_V}{2\sqrt{N_c}\hat{e}_f} f_L(z) e^{-\omega_L^2 r^2/2}, \quad (31)$$

for the DGKP longitudinal meson light-cone wave function. $\hat{e}_f$ is the effective charge arising from the sum over quark flavors in the meson: $\hat{e}_f = 1/\sqrt{2}, 1/3$, and $2/3$ for the ρ, ϕ and J/Ψ, respectively. Similarly, the DGKP transverse meson light-cone wave functions can be written as

$$\Psi_{h,\bar{h}}^{V,T(\gamma=\pm)}(r,z) = \pm\left(\frac{i\omega_T^2 r e^{\pm i\theta_r}}{M_V} [z\,\delta_{h\pm,\bar{h}\mp} - (1-z)\,\delta_{h\mp,\bar{h}\pm}] + \frac{m_f}{M_V}\delta_{h\pm,\bar{h}\pm} \right) \frac{\sqrt{\pi} f_V}{\sqrt{2N_c}\hat{e}_f} f_T(z) e^{-\omega_T^2 r^2/2}. \quad (32)$$

The normalization condition (22) on the DGKP wave function leads to the relations

$$\omega_\lambda = \frac{\pi f_V}{\sqrt{2N_c}\hat{e}_f}\sqrt{I_\lambda}, \quad (33)$$

with

$$I_L = \int_0^1 dz z^2 (1-z)^2 f_L^2(z), \quad (34)$$

and

$$I_T = \int_0^1 dz \frac{[z^2+(1-z)^2]\omega_T^2 + m_f^2}{M_V^2} f_T^2(z). \quad (35)$$

The leptonic decay width constraints (26) and (27) on the DGKP wave function yield

$$1 = \int_0^1 dz z(1-z) f_L(z) = \int_0^1 dz \frac{2[z^2+(1-z)^2]\omega_T^2 + m_f^2}{2M_V^2 z(1-z)} f_T(z). \quad (36)$$

The values of ω_λ and $\mathcal{N}_\lambda$ are found by solving Eqs. (33) and (36) simultaneously, and are given in Table II. The values of the decay constants used are the central experimental values [25]: $f_\rho = 0.153 \pm 0.004$ GeV, and $f_\phi = 0.079 \pm 0.001$ GeV.

The resulting behavior of the ρ wave functions is shown for the case of the FKS quark masses in Fig. 3. As is clear from Eqs. (28)–(32), the wave functions peak at $z = 0.5$ and $r = 0$, and go rapidly to zero as $z \to 0,1$ and $r \to \infty$, so that large dipoles are suppressed. From the figures, we see that the transverse wave function has a broader distribution than the longitudinal wave function. The ϕ wave functions are qualitatively similar to, but slightly more sharply peaked than, the ρ wave functions.

The GW model uses a much smaller value for the light quark masses than the FKS model, as we saw in Sec. II C. We might expect this to have a striking effect on the transverse wave function of the ρ, since the transverse wave function (32) vanishes at $r = 0$ for zero quark masses, while the longitudinal wave function (31) does not. The transverse DGKP wave function with the light quark mass used in the GW dipole model is shown in Fig. 4 for the ρ. As can be seen, the smaller quark mass decreases the wave function at the origin and shifts the peak to slightly larger r.

[8] Note that the theoretical analysis of Halperin and Zhitnitsky [23] shows that such a factorizing ansatz must break down at the end points of z. However, since the latter are suppressed in the DGKP wave function, this has no practical consequence.

[9] DGKP do not actually include the factor $z(1-z)$ in the scalar wave function. This is because they define the scalar wave function to be the right-hand side of Eq. (15) divided by $z(1-z)$.

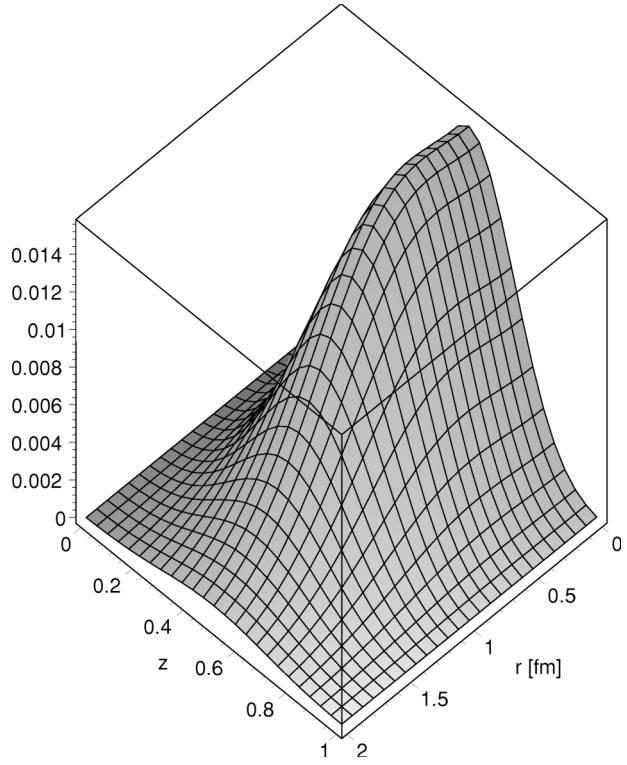

FIG. 4. The ρ wave function $|\Psi^T|^2$ in the DGKP model with the quark mass used in the GW dipole model.

B. Boosted wave functions

In this approach the scalar part of the wave function is obtained by taking a given wave function in the meson rest frame. This is then ''boosted'' into a light-cone wave function using the Brodsky-Huang-Lepage prescription, in which the expressions for the off-shellness in the center-of-mass and light-cone frames are equated [26] (or equivalently, the expressions for the invariant mass of the $q\bar{q}$ pair in the center-of-mass and light-cone frames are equated [27]).

The simplest version of this approach assumes a simple Gaussian wave function in the meson rest frame. Alternatively NNPZ [10] have supplemented this by adding a hard ''Coulomb'' contribution in the hope of improving the description of the rest frame wave function at small r. We refer to [10] for details of this procedure. Here we simply state the result, which is that the NNPZ meson light-cone wave functions are given by Eqs. (24),(25) with $\delta=1$, where the scalar wave functions $\phi_\lambda(r,z)$ are taken to be a sum of a soft (Gaussian in the rest frame) part and a hard (Coulomb) part:

$$\phi_\lambda(r,z)=\mathcal{N}_\lambda\Bigg[4z(1-z)\sqrt{2\pi R^2}\exp\left(-\frac{m_f^2R^2}{8z(1-z)}\right)\times\exp\left(-\frac{2z(1-z)r^2}{R^2}\right)\exp\left(\frac{m_f^2R^2}{2}\right)+16C^4\frac{a^3(r)}{A(r,z)B^3(r,z)}rK_1[A(r,z)r/B(r,z)]\Bigg]. \tag{37}$$

Here

$$A(r,z)=\sqrt{1+\frac{C^2a^2(r)m_f^2}{z(1-z)}-4C^2a^2(r)m_f^2}, \tag{38}$$

$$B(r,z)=\frac{Ca(r)}{\sqrt{z(1-z)}}, \tag{39}$$

and

$$a(r)=\frac{3}{4m_f\alpha_s(r)} \tag{40}$$

is a running Bohr radius. The strong coupling α_s is chosen to run according to the prescription [28,22]

$$\alpha_s=\alpha_0 \quad \text{for} \quad r>r^s$$

and

$$\alpha_s(r)=\frac{4\pi}{\beta_0\log(1/(\Lambda_{\rm QCD}^2r^2))} \quad \text{for} \quad r<r^s, \tag{41}$$

where $r^s=0.42$ fm, $\alpha_0=0.8$, $\Lambda_{\rm QCD}=0.2$ GeV and $\beta_0=(33-2n_f)/3$. Apart from the normalization constants $\mathcal{N}_\lambda$, these wave functions depend on two free parameters which are independent of the meson helicity: a ''radius'' parameter R and a parameter C, introduced to control the transition between the hard Coulomb-like interaction and the soft confining interaction in the rest-frame wave function. The case of a simple Gaussian wave function in the rest frame, which we will refer to as a ''boosted Gaussian wave function'' can be obtained by simply setting $C=0$ (we still choose $\delta=1$ when considering this wave function).

At this point we comment on two issues associated with the behavior of the Coulomb part of the scalar wave function for small r. The first is that (37) diverges logarithmically as

TABLE III. Parameters of the NNPZ light-cone wave functions in appropriate GeV based units, together with the resulting values for the decay constants f_V. Where two values are given, the first and second values are for the FKS and GW quark masses, respectively.

NNPZ	R^2	C	$\mathcal{N}_L$	$\mathcal{N}_T$	$f_V(L)$	$f_V(T)$
ρ	25.0	0.36	0.0123,0.0121	0.0125,0.0137	0.143,0.147	0.157,0.109
ϕ	18.0	0.53	0.0122,0.0124	0.0124,0.0131	0.078,0.078	0.087,0.067

TABLE IV. Parameters of the boosted Gaussian wave function in appropriate GeV based units, together with the resulting values for the decay constants f_V. Where two values are given, the first and second values are for the FKS and GW quark masses, respectively.

Gaussian	R^2	$\mathcal{N}_L$	$\mathcal{N}_T$	$f_V(L)$	$f_V(T)$
ρ	12.3	0.0213,0.0244	0.0221,0.0259	0.153,0.161	0.203,0.192
ϕ	10.0	0.0214,0.0243	0.0219,0.0251	0.075,0.079	0.095,0.088

$r\to 0$ at $z=0.5$. This divergence is, however, regulated in observables. For example, while the resulting squared wave functions $|\Psi^{V(\lambda)}|^2$ exhibit a narrow, singular peak at $r=0,z=0.5$, the quantity $r|\Psi^{V(\lambda)}|^2$ which enters the normalization condition (22) is zero in this limit. Nevertheless, this singular behavior does have a (finite) effect when computing the meson decay constant which depends upon the behavior of the wave function at $r=0$. The second issue is that when the scalar wave function (37) is substituted into Eqs. (24)–(27), the derivatives in r give rise to inverse power divergences at $r=0$ when acting upon the running coupling (41). However, these divergences occur solely in terms which are strictly higher order in α_s. Henceforth we discard these higher order terms, which is equivalent to omitting all derivatives of $\alpha_s(r)$ with respect to r when differentiating the scalar wave function (37). We stress that none of these issues arise when using the boosted Gaussian wave function.

It remains to determine the various constants. NNPZ [10] determined both R and C by using a standard variational procedure for the initial center-of-mass wave function using a non-relativistic potential. They then checked that the resulting predictions (23) were in reasonable accord with the observed leptonic decay widths.[10] Here we follow a slightly modified procedure, since we want to be able to easily adjust the quark masses to those assumed in the various dipole models. Specifically, we fixed C at the value chosen by NNPZ and vary the value of R to give approximate agreement with the decay width constraints (23). In practice, we found it adequate to use the same R value for both the FKS and GW mass choices. The resulting values of R and C, with the associated values of the normalization constants, are shown in Table III, and are not very different from the original parameters of NNPZ. In addition we show the results for the boosted Gaussian case ($C=0$) in Table IV.

The behavior of the resulting ρ wave functions is shown in Figs. 5 and 6 with the FKS choice of quark masses. The divergence at $r=0,z=0.5$ is not visible since we do not plot down to $r=0$. Like the DGKP wave functions, they peak at $z=0.5$ and $r=0$, and go rapidly to zero as $z\to 0,1$ and $r\to\infty$. However, on comparing these figures with each other, and with Fig. 3, two clear differences emerge.

Firstly, the peak in z is less sharp in the boosted Gaussian case than in the DGKP and NNPZ cases. Secondly, the large difference between the longitudinal and transverse wave functions found in the DGKP case is much less marked in the NNPZ and boosted Gaussian wave functions. In both cases, the peak in the transverse wave function is still broader than that in the longitudinal wave function, but it is a small effect in comparison with the DGKP case. This presumably reflects the fact that in the NNPZ and boosted Gaussian wave functions, the parameter R has the same value for both helicities, since both wave functions are generated from the same non-relativistic wave function by the Brodsky-Huang-Lepage procedure.

IV. REAL PARTS, SLOPE PARAMETERS AND CROSS SECTIONS

We now have all the ingredients required to calculate the absorptive parts (2) of the forward amplitudes for vector meson production. For the case of the NNPZ wave functions, we substitute the photon wave functions[11] (19),(20) and the vector meson wave functions (24),(25) with $\delta=1$ into (2). Summing over the quark/antiquark helicities and averaging over the transverse polarization states of the photon, we obtain[12]

$$\mathfrak{Im}\mathcal{A}^L_{\rm NNPZ}=s\frac{N_c\hat{e}_f\sqrt{4\pi\alpha_{\rm em}}}{(2\pi)^2}\frac{2Q}{M_V}\int d^2\boldsymbol{r}\hat{\sigma}(s,r)\times\int_0^1 dz\{[m_f^2+z(1-z)M_V^2]K_0(\epsilon r)\phi_L(r,z)-K_0(\epsilon r)\nabla_r^2)\phi_L(r,z)\} \tag{42}$$

$$\mathfrak{Im}\mathcal{A}^T_{\rm NNPZ}=s\frac{N_c\hat{e}_f\sqrt{4\pi\alpha_{\rm em}}}{(2\pi)^2}\int d^2\boldsymbol{r}\hat{\sigma}(s,r)\int_0^1\frac{dz}{z(1-z)}\times\{[z^2+(1-z)^2]\partial_r K_0(\epsilon r)\partial_r\phi_T(r,z)+m_f^2K_0(\epsilon r)\phi_T(r,z)\}, \tag{43}$$

where $\phi_{L,T}(r,z)$ are given by Eq. (37). Similarly, using the DGKP wave functions (31) and (32), we obtain

[10]Note that a shortcoming of this model is that Eqs. (23)–(25) give slightly different predictions for the decay constant for the case of transverse and longitudinal meson helicities, because NNPZ use helicity independent values of R,C.

[11]For the FKS case, we must also include the effect of the enhancemect factor (7).

[12]These results reduce to Eq. (8) of [10] if, in Eq. (42), we integrate the second term by parts assuming an r-independent dipole cross section.

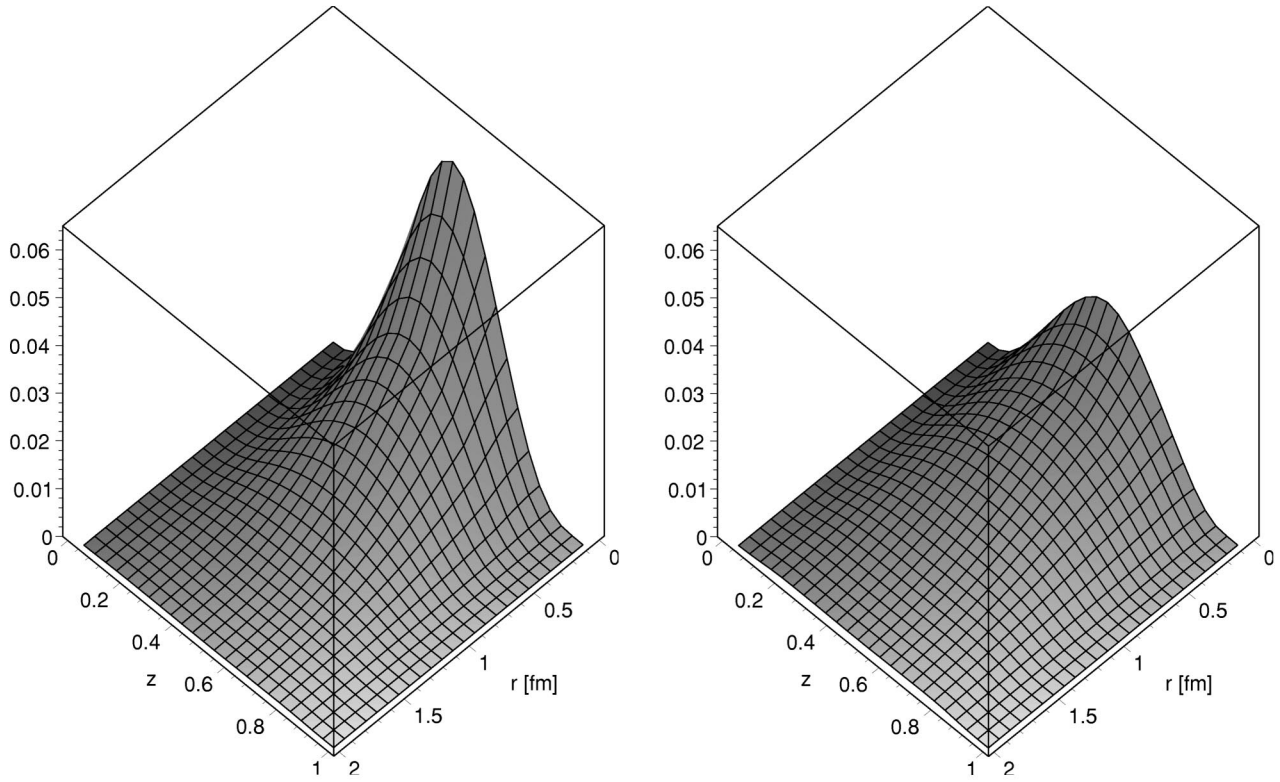

FIG. 5. The ρ wave functions $|\Psi^L|^2$ (left) and $|\Psi^T|^2$ (right) in the NNPZ model with the quark mass used in the FKS dipole model.

$$\Im\mathrm{m}\mathcal{A}^L_{\mathrm{DGKP}} = s\int d^2\boldsymbol{r}\hat{\sigma}(s,r)\int_0^1 dz\,\sqrt{\frac{\alpha_{\mathrm{em}}}{4\pi}}f_V z(1-z) \times f_L(z)e^{-\omega_L^2 r^2/2}2z(1-z)QK_0(\epsilon r), \quad (44)$$

$$\Im\mathrm{m}\mathcal{A}^T_{\mathrm{DGKP}} = s\int d^2\boldsymbol{r}\hat{\sigma}(s,r)\int_0^1 dz\,\sqrt{\frac{\alpha_{\mathrm{em}}}{4\pi}}f_V f_T(z)e^{-\omega_T^2 r^2/2} \times\left(\frac{\omega_T^2\epsilon r}{M_V}[z^2+(1-z)^2]K_1(\epsilon r)+\frac{m_f^2}{M_V}K_0(\epsilon r)\right). \quad (45)$$

So far, we have focussed on the imaginary amplitude. Taking into account the real part contribution, the differential cross section is given by

$$\left.\frac{d\sigma^{T,L}}{dt}\right|_{t=0} = \frac{1}{16\pi s^2}|\Im\mathrm{m}\mathcal{A}^{T,L}|^2(1+\beta^2), \quad (46)$$

where β is the ratio of real to imaginary parts of the amplitude. It is most straightforward to reconstruct the real part of the amplitude in the FKS dipole model, where the dipole cross section (3), and hence the amplitude (2), is given as the sum of hard and soft Regge pole terms. In this case, the real part is given by

$$\Re\mathrm{e}\mathcal{A}_{\mathrm{FKS}} = -\Im\mathrm{m}\mathcal{A}_{\mathrm{soft}}\cot\left(\frac{\pi\alpha_S}{2}\right)-\Im\mathrm{m}\mathcal{A}_{\mathrm{hard}}\cot\left(\frac{\pi\alpha_H}{2}\right), \quad (47)$$

where $\alpha_{S,H}=1+\lambda_{S,H}=1.06,1.44$ and $\Im\mathrm{m}\mathcal{A}_{\mathrm{soft}}$ and $\Im\mathrm{m}\mathcal{A}_{\mathrm{hard}}$ are the contributions from the soft and hard Pomeron pieces of FKS dipole cross section (3), respectively.

It follows from (47) that, in the FKS model, β lies between 0.09 and 0.83, corresponding to pure soft and hard Pomeron dominance, respectively; within this range, the value of β reflects directly the relative importance of the hard Pomeron. Other things being equal, β will therefore increase with increasing energy, because the hard term in the dipole cross section increases more rapidly with energy than the soft term. It will also increase with Q^2, because the hard term is dominant for small dipoles, which are increasingly explored as Q^2 increases. These features are illustrated in Fig. 7, which shows the values of β obtained as functions of W and Q^2 obtained using the DGKP wave functions. Here we also see that β is larger for the longitudinal than for the transverse case, reflecting sharper peaking of the longitudinal vector meson wave functions. Similar results for the real parts are obtained using the NNPZ wave functions.

From the above figures, we see that while the corrections from the real parts in the cross section formulas (46) are clearly significant in some kinematic ranges, they are nowhere dominant. Because of this and because the ratio β is

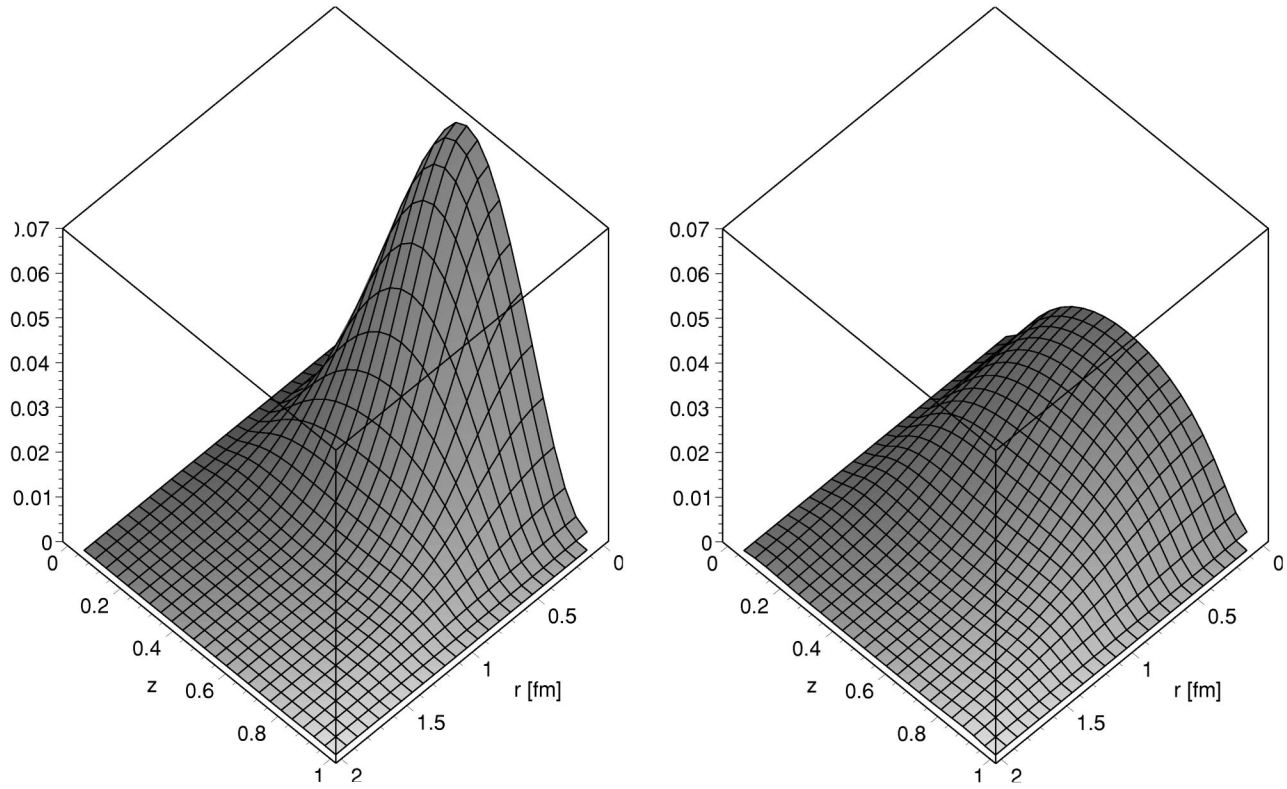

FIG. 6. The ρ wave functions $|\Psi^L|^2$ (left) and $|\Psi^T|^2$ (right) in the boosted Gaussian model with the quark mass used in the FKS dipole model.

expected to be similar in the different models,[13] we shall use the estimates (47) of the ratio β obtained in the FKS model in all dipole models.

Assuming the usual exponential ansatz for the t dependence, the total cross sections are given by

$$\sigma^{T,L}(\gamma^* p \to Vp) = \frac{d\sigma^{T,L}/dt|_{t=0}}{B}. \tag{48}$$

Unfortunately, the values of the slope parameter B are not very accurately measured. Here we use a parametrization

$$B = 0.60\left(\frac{14}{(Q^2+M_V^2)^{0.26}}+1\right) \tag{49}$$

obtained from a fit to experimental data by Mellado [29], and used in their analysis of the predictions of the GW dipole model by Caldwell and Soares [30]. The resulting values for B are shown in Fig. 8, where we also show the results of an alternative parametrization of Kreisel [31] to illustrate the range of values that can be obtained from different fits to the data. When comparing the predictions of (48) for the vector meson cross sections with data, it is important to bear in mind that this uncertainty in the input value of the slope parameter can easily introduce errors up to of order 30% or so and that, within this range, this error may be Q^2 dependent.

Finally, on comparing with experimental data, we show $\sigma^{\rm TOT} = \sigma^T + \epsilon\sigma^L$ with $\epsilon = 0.98$ in all our plots, although the HERA data range from 0.96 to 1.00.

V. RESULTS

In this section we will compare the predictions of the three dipole models with the experimental data for our three choices of the vector meson wave function, without any adjustment of parameters. Before doing so, however, we emphasize again that the uncertainty in the slope parameter can give rise to Q^2-dependent errors of up to 30% in the cross section, which should be borne in mind when comparing with experiment. This effect should, hopefully, be much smaller in the ratio R. However, it ought not to be completely negligible since the longitudinal and transverse cross sections will presumably have slightly different slope parameters, as to some degree they explore dipoles of different sizes.

A. ρ meson production

The predictions of the FKS model for the Q^2 dependence of the cross section and for the longitudinal to transverse ratio R are shown in Fig. 9 for the three different wave func-

[13]This was confirmed explicitly for two distinct dipole models in [3].

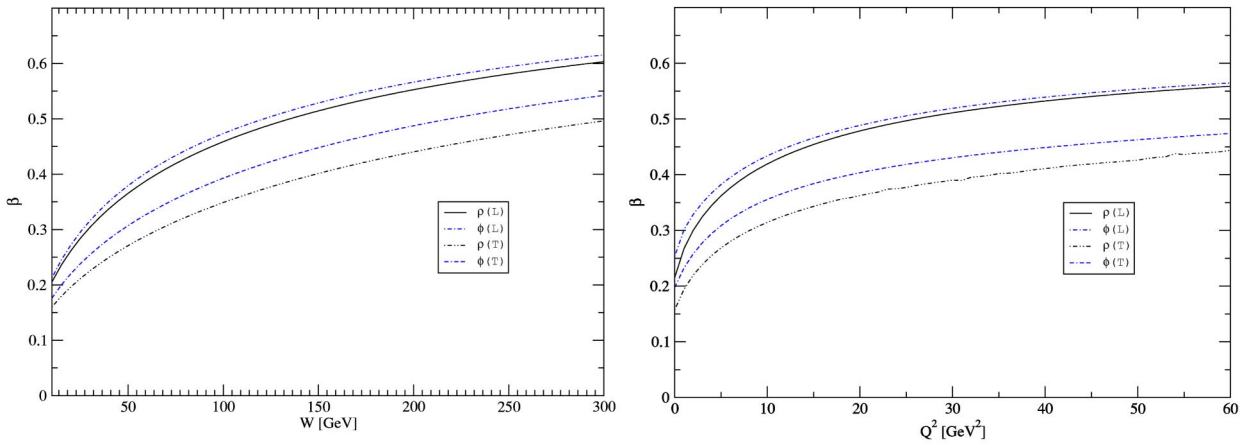

FIG. 7. Left: W dependence of the ratio β of the real to imaginary part of the forward amplitude in the FKS model, using the DGKP wave functions, for $Q^2 = 10$ GeV^2. Right: Q^2 dependence of β in the FKS model, using the DGKP wave functions, for $W = 75$ GeV.

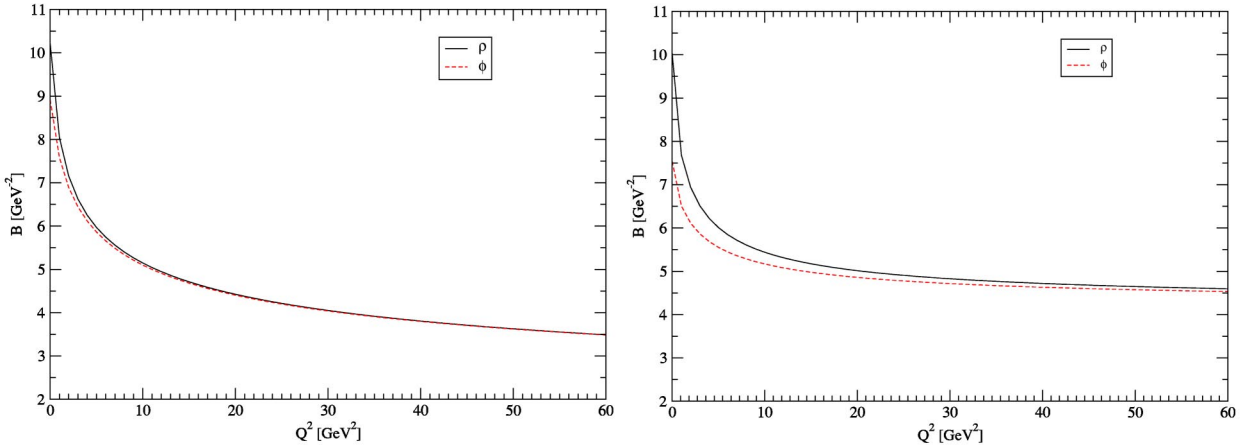

FIG. 8. Left: Parametrization of the slope B by Mellado [29] for the ρ and ϕ. Right: Parametrization of the slope B by Kreisel [31] for the ρ and ϕ.

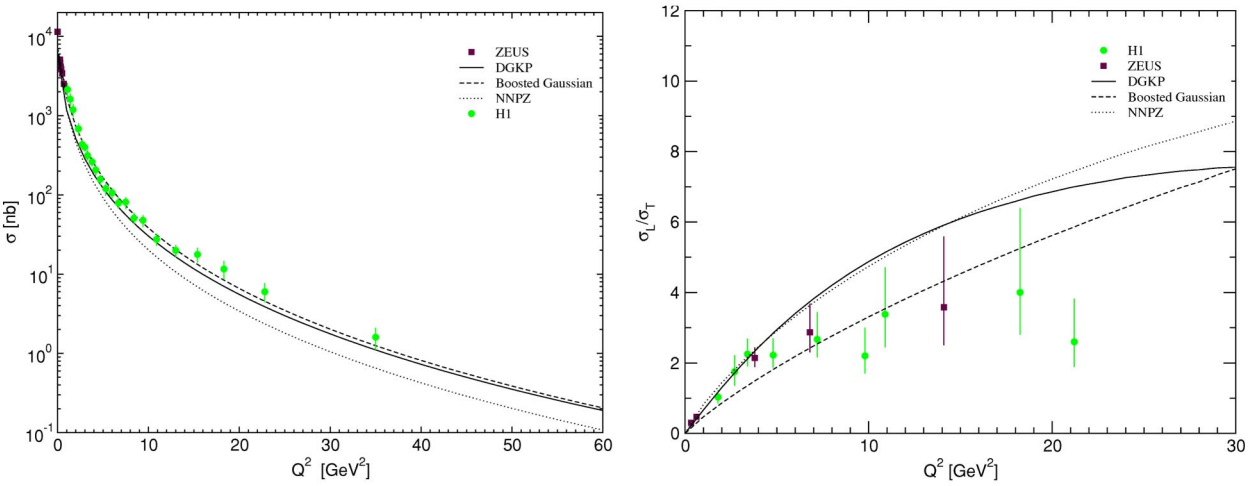

FIG. 9. The Q^2 dependence of (left) the total cross section and (right) the longitudinal to transverse cross section ratio for ρ production at $W = 75$ GeV in the FKS model using the three different meson wave functions. Data from (left) [32,34] and (right) [32,33].

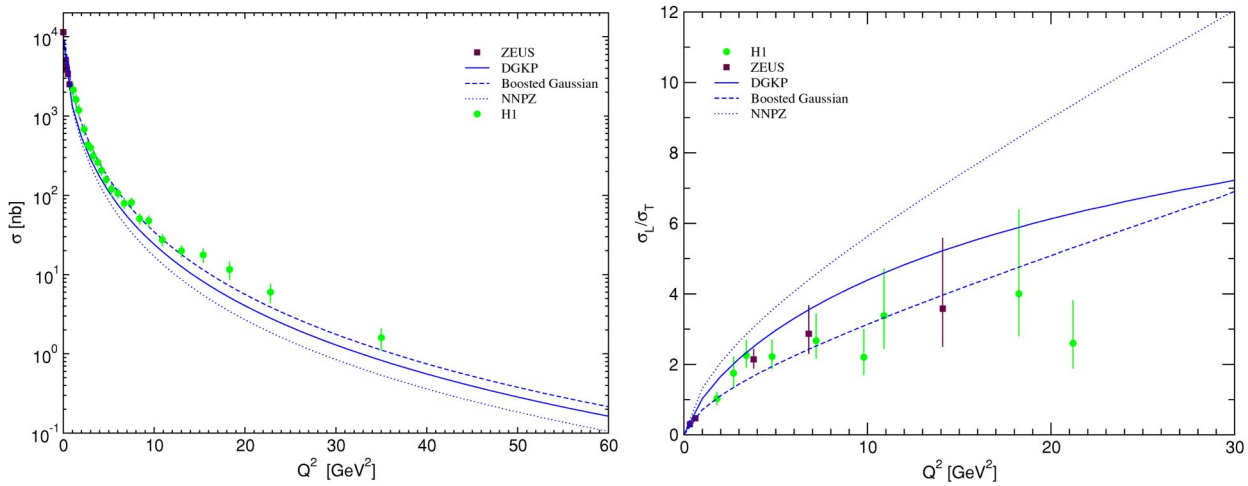

FIG. 10. The Q^2 dependence of (left) the total cross section and (right) the longitudinal to transverse cross section ratio for ρ production at $W=75$ GeV in the GW model using the three different meson wave functions. Data from (left) [32,34] and (right) [32,33].

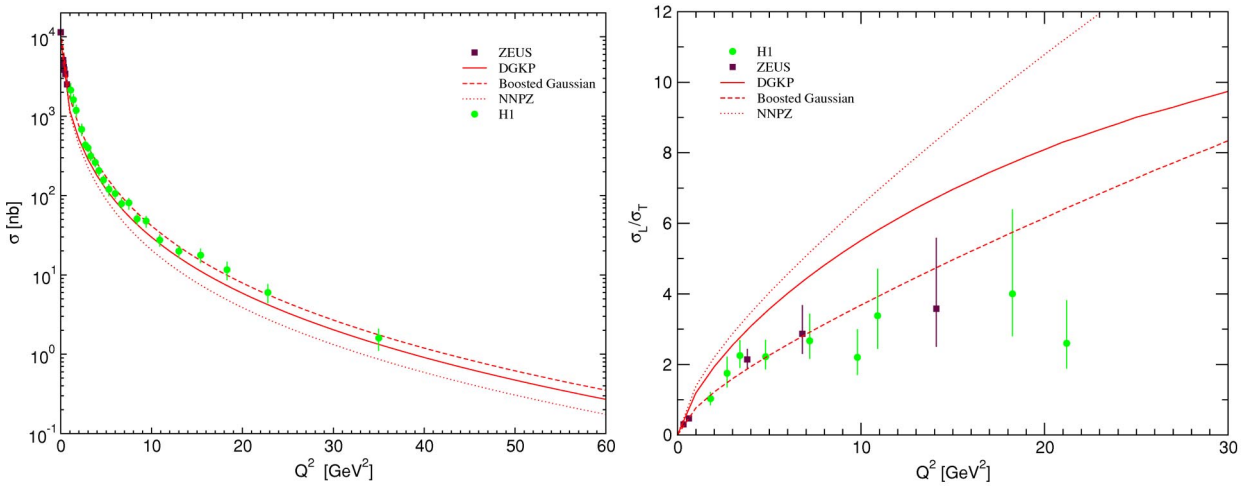

FIG. 11. The Q^2 dependence of (left) the total cross section and (right) the longitudinal to transverse cross section ratio for ρ production at $W=75$ GeV in the CGC model using the three different meson wave functions. Data from (left) [32,34] and (right) [32,33].

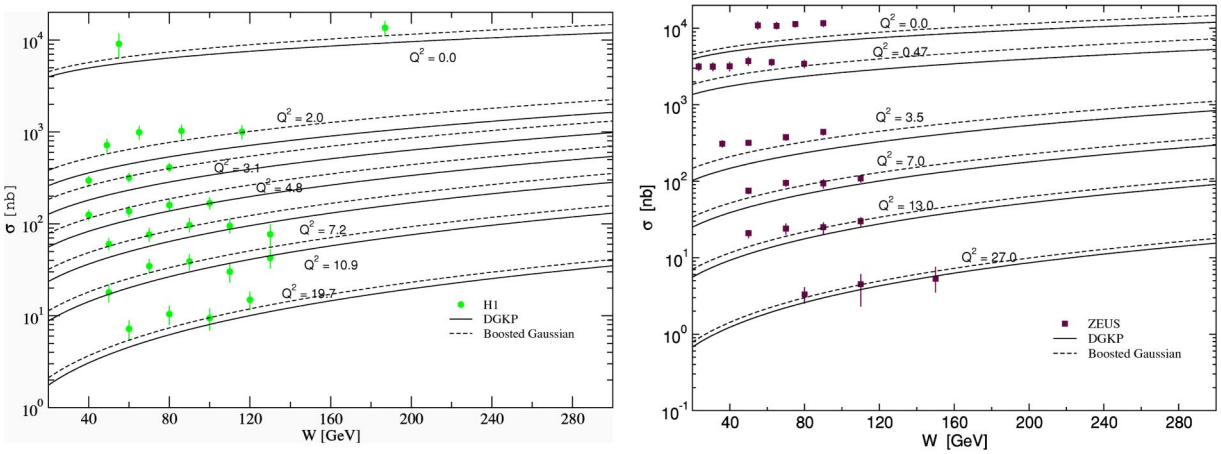

FIG. 12. The W dependence of the total cross section for ρ production at various values of Q^2. We use the FKS dipole model and compare the boosted Gaussian and DGKP wave functions. Data from (left) [34] and (right) [32].

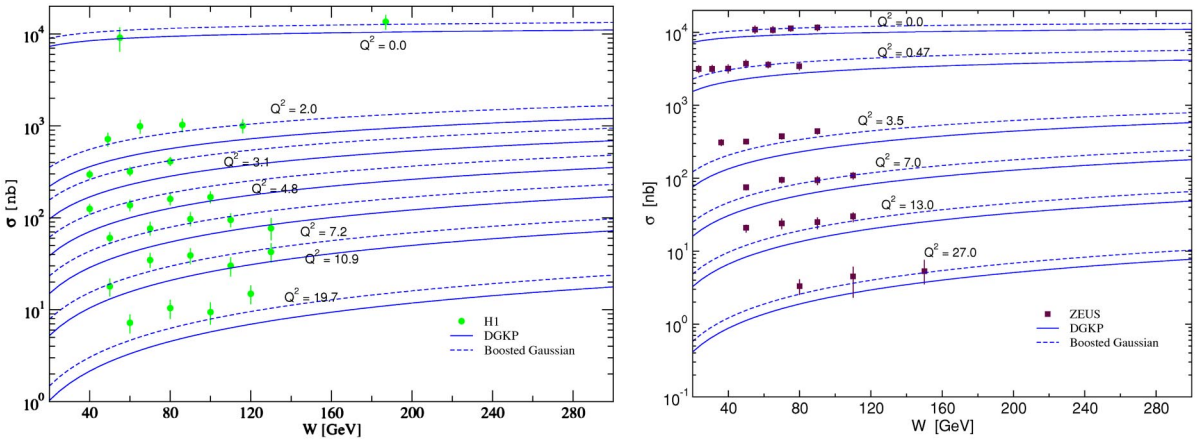

FIG. 13. The W dependence of the total cross section for ρ production at various values of Q^2. We use the GW dipole model and compare the boosted Gaussian and DGKP wave functions. Data from (left) [34] and (right) [32].

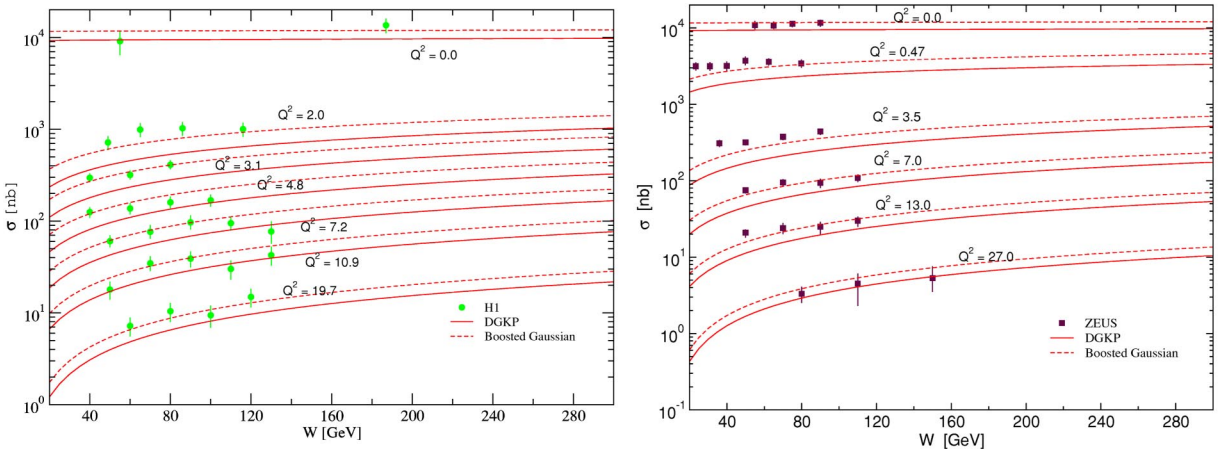

FIG. 14. The W dependence of the total cross section for ρ production at various values of Q^2. We use the CGC dipole model and compare the boosted Gaussian and DGKP wave functions. Data from (left) [34] and (right) [32].

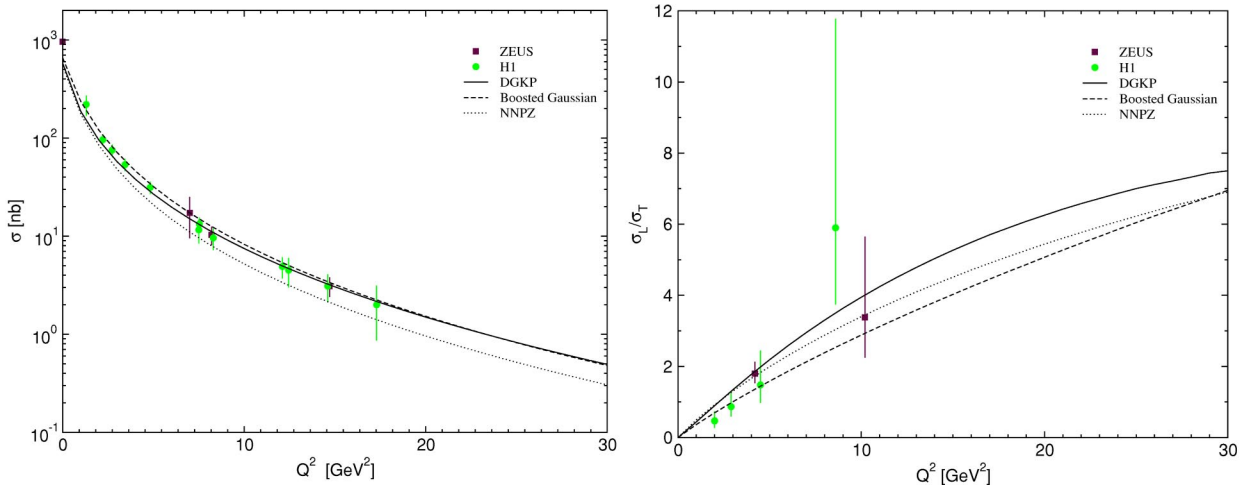

FIG. 15. The Q^2 dependence of (left) the total cross section and (right) the longitudinal to transverse cross section ratio for ϕ production at $W=90$ GeV in the FKS model using the three different meson wave functions. Data from (left) [35,36] and (right) [37,38].

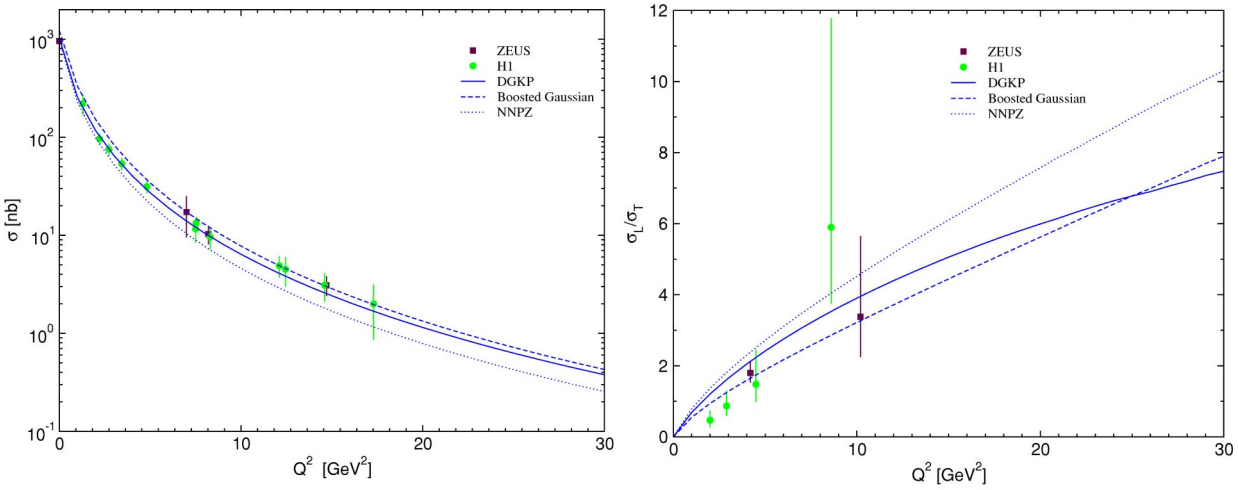

FIG. 16. The Q^2 dependence of (left) the total cross section and (right) the longitudinal to transverse cross section ratio for ϕ production at $W=90$ GeV in the GW model using the three different wave functions. Data from (left) [35,36] and (right) [37,38].

tions considered. The equivalent plots for the GW and CGC model are in Figs. 10 and 11, respectively.

The ZEUS total cross-section data are at the following center-of-mass energies: $Q^2=0$ GeV^2, $W=75$ GeV, otherwise $W=51.1$ GeV. The H1 total cross-section data are at $W=75$ GeV. The H1 data on the longitudinal to transverse ratio are for $Q^2=9.8, 18.25$ GeV^2, in the range 40 GeV $<W<140$ GeV, otherwise they are at $W=75$ GeV. Similarly, the ZEUS data are for $Q^2=0.33$ and 0.62 GeV^2, at $W=47$ GeV, otherwise at $W=67$ GeV. For the theory curves we always take $W=75$ GeV.

For all three dipole models, the data favor the boosted Gaussian wave function, whilst the DGKP wave function produces reasonable agreement for FKS and is rather less satisfactory for the GW and CGC models. The NNPZ wave function is well below the total cross section data for all three models and, for the GW and CGC models, in disagreement with the data on the longitudinal to transverse ratio. However, as noted in Sec. III B, although the spurious singularity in this wave function does not contribute directly to the predicted cross sections, it influences them indirectly because it influences the value of the radial parameter R deduced from the decay width. In what follows, we will therefore focus on the DGKP and boosted Gaussian wave functions.

Figures 12, 13, and 14 show the W dependence at fixed values of Q^2 for the ρ meson. Apart from the normalization, the W dependence is good in all cases. The normalization is best described by the boosted Gaussian wave function. With this wave function, the FKS model is in reasonably good agreement with the data, except for the ZEUS data at very low Q^2; while the GW and CGC models give reasonable agreement everywhere.

This last comment contrasts somewhat with the work of Caldwell and Soares [30], who have already presented predictions for the GW model using a boosted Gaussian wave function. These authors also found good agreement with the data on the longitudinal to transverse ratio and with the W dependence at fixed Q^2 apart from the normalization. However, their results for the normalization, and hence, implicitly, for the Q^2 dependence of the production cross section, were relatively poor. However, these authors did not implement the leptonic decay width constraint but fixed the radial parameter R in the boosted Gaussian by requiring that the exponential in R of the wave function gives a value of $1/e$ when the $q\bar{q}$ invariant mass is equal to the meson's mass. This yielded $R^2=15.5$ GeV^{-2} for ρ and $R^2=8.3$ GeV^{-2} for ϕ compared to our values shown in Table IV. In addition, they neglected real parts, which can result in a 20% reduction in the cross section for large Q^2.

B. ϕ meson production

The corresponding plots to those in the previous section are repeated for the ϕ meson in Figs. 15, 16 and 17. The H1 total cross section data are at the following center-of-mass energies: for $Q^2=7.5,8.3,12.5,14.6,17.3$ GeV^2, $W=100$ GeV, otherwise $W=75$ GeV. Similarly for the ZEUS data, for $Q^2=0.0,8.2,14.7$ GeV^2, $W=70,94,99$ GeV, respectively. The H1 data on the longitudinal to transverse ratio are in the range 40 GeV$<W<$130 GeV. Similarly the ZEUS data are in the range 25 GeV$<W<$120 GeV. For the theory curves we always take $W=90$ GeV.

The situation is rather similar, as one might expect, to that of the ρ, i.e. all three dipole models tend to do rather well with either of the DGKP or boosted Gaussian wave functions, while the NNPZ wave function is less satisfactory.

VI. CONCLUSIONS

We have performed a detailed study, comparing the predictions on ρ and ϕ meson electroproduction arising from three different models of the meson wave function in combination with three different models for the fundamental dipole cross section. Our results are broadly encouraging and support the use of the dipole approach.

The data can be explained rather well using the dipole model of Forshaw, Kerley and Shaw, or those of Golec-

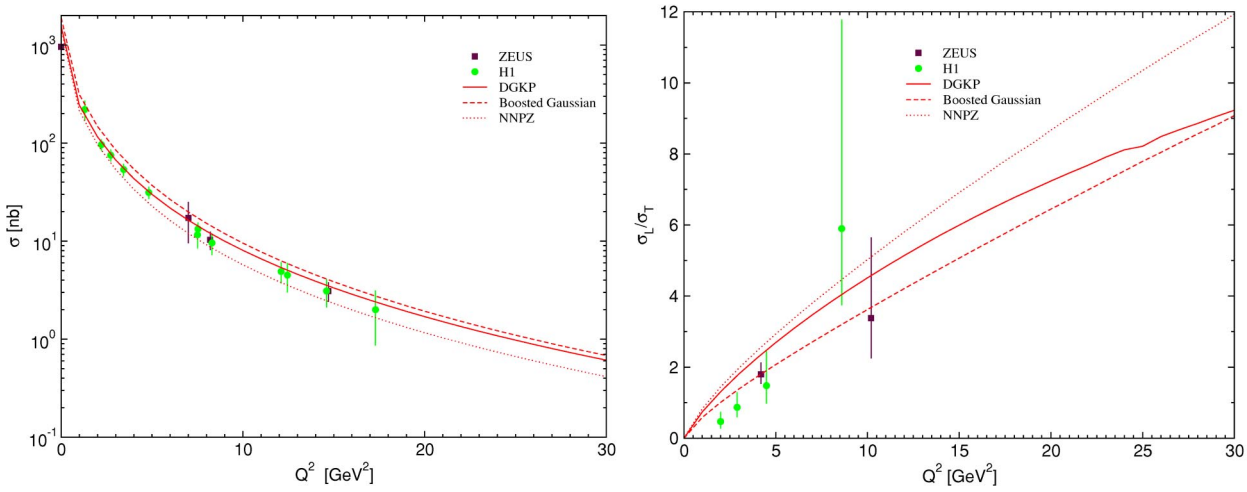

FIG. 17. The Q^2 dependence of (left) the total cross section and (right) the longitudinal to transverse cross section ratio for ϕ production at $W=90$ GeV in the CGC model using the three different wave functions. Data from (left) [35,36] and (right) [37,38].

Biernat and Wüsthoff and of Iancu, Itakura and Munier, in conjunction with either the boosted Gaussian or DGKP meson wave function. Certainly, we anticipate that excellent agreement could be obtained if one decided to tune the meson wave functions. Note that agreement extends to the ratio of longitudinal to transverse meson production. The NNPZ wave function, which has, as noted, an unphysical singularity at $z=0.5$, $r=0$, is not so successful.

For the future, it is clear that one could use the high quality data from HERA to constrain the meson wave functions provided the dipole cross section is sufficiently constrained.

ACKNOWLEDGMENTS

This research was supported in part by the U.K. Particle Physics and Astronomy Research Council. We should like to thank S. Munier, M. Soares, and A. Stasto for useful discussions. We also thank M. V. T. Machado for useful comments on the text.

[1] J.R. Forshaw, G. Kerley, and G. Shaw, Phys. Rev. D **60**, 074012 (1999).
[2] J.R. Forshaw, G. Kerley, and G. Shaw, Nucl. Phys. **A675**, 80c (2000).
[3] M. McDermott, R. Sandapen, and G. Shaw, Eur. Phys. J. C **22**, 655 (2002).
[4] H1 Collaboration, C. Adloff *et al.*, Z. Phys. C **76**, 613 (1997); ZEUS Collaboration, J. Breitweg *et al.*, Eur. Phys. J. C **6**, 43 (1999).
[5] H1 Collaboration, C. Adloff *et al.*, Phys. Lett. B **517**, 47 (2001); S. Chekanov *et al.*, *ibid.* **573**, 46 (2003).
[6] K. Golec-Biernat and M. Wüsthoff, Phys. Rev. D **59**, 014017 (1999).
[7] K. Golec-Biernat and M. Wüsthoff, Phys. Rev. D **60**, 114023 (1999).
[8] E. Iancu, K. Itakura, and S. Munier, hep-ph/0310338.
[9] H.G. Dosch, T. Gousset, G. Kulzinger, and H.J. Pirner, Phys. Rev. D **55**, 2602 (1997).
[10] J. Nemchik, N.N. Nikolaev, E. Predazzi, and B.G. Zakharov, Z. Phys. C **75**, 71 (1997).
[11] N.N. Nikolaev and B.G. Zakharov, Z. Phys. C **49**, 607 (1991); **53**, 331 (1992); A.H. Mueller, Nucl. Phys. **B415**, 373 (1994); A.H. Mueller and B. Patel, *ibid.* **B425**, 471 (1994).
[12] M. McDermott, "The dipole picture of small x physics (A summary of the Amirim meeting)," hep-ph/0008260v2.
[13] L. Frankfurt, V. Guzey, and M. Strikman, Phys. Rev. D **58**, 094039 (1998).
[14] H. Fraas, B.J. Read, and D. Schildknecht, Nucl. Phys. **B86**, 346 (1975).
[15] G. Shaw, Phys. Rev. D **47**, R3676 (1993); Phys. Lett. B **228**, 125 (1989); P. Ditsas and G. Shaw, Nucl. Phys. **B113**, 246 (1976).
[16] G. Cvetic, D. Schildknecht, B. Surrow, and M. Tentyukov, Eur. Phys. J. C **20**, 77 (2001).
[17] L.V. Gribov, E.M. Levin, and M.G. Ryskin, Phys. Rep. **100**, 1 (1983).
[18] J.R. Forshaw, G. Kerley, and G. Shaw, *Proceedings of the 8th International Workshop on Deep Inelastic Scattering*, edited by J.A. Gracey and T. Greenshaw (World Scientific, Singapore, 2001).
[19] J. Bartels, K. Golec-Biernat, and H. Kowalski, Phys. Rev. D **66**, 014001 (2002).
[20] S.J. Brodsky and G.P. Lepage, Phys. Rev. D **22**, 2157 (1980).
[21] A. Hebecker and P.V. Landshoff, Phys. Lett. B **419**, 393 (1998).
[22] S. Munier, A. Mueller, and A. Stasto, Nucl. Phys. **B603**, 427 (2001).
[23] I. Halperin and A. Zhitnitsky, Phys. Rev. D **56**, 184 (1997).
[24] M. Wirbel, B. Stech, and M. Bauer, Z. Phys. C **29**, 637 (1985).

[25] Particle Data Group, K. Hagiwara *et al.*, Phys. Rev. D **66**, 010001 (2002).
[26] S.J. Brodsky, T. Huang and G.P. LePage, shorter version contributed to 20th International Conference on High Energy Physics, Madison, Wisconsin, 1980, SLAC-PUB-2540.
[27] A. Donnachie, J. Gravelis, and G. Shaw, Phys. Rev. D **63**, 114013 (2001).
[28] J. Nemchik, N.N. Nikolaev, and B.G. Zakharov, Phys. Lett. B **341**, 228 (1994).
[29] B. Mellado, result given in [30].
[30] A. Caldwell and M. Soares, Nucl. Phys. **A696**, 125 (2001).
[31] A. Kreisel, paper presented at LISHEP 02, hep-ex/020801v1.
[32] ZEUS Collaboration, J. Breitweg *et al.*, Eur. Phys. J. C **6**, 603 (1999).
[33] H1 Collaboration, S. Aid *et al.*, Nucl. Phys. **B463**, 3 (1996).
[34] H1 Collaboration, C. Adloff *et al.*, Eur. Phys. J. C **13**, 371 (2000); H1 Collaboration, S. Aid *et al.*, Nucl. Phys. **B468**, 3 (1996).
[35] H1 Collaboration, C. Adloff *et al.*, Phys. Lett. B **483**, 360 (2000); Z. Phys. C **75**, 607 (1997).
[36] ZEUS Collaboration, M. Derrick *et al.*, Phys. Lett. B **377**, 259 (1996); **380**, 220 (1996).
[37] H1 Collaboration, C. Adloff *et al.*, Phys. Lett. B **483**, 360 (2000).
[38] ZEUS Collaboration (unpublished).